Journal of Power Sources 218 (2012) 445–454

Contents lists available at SciVerse ScienceDirect

Journal of Power Sources

journal homepage: www.elsevier.com/locate/jpowsour

A mechanistic-based healing model for self-healing glass seals used in solid oxide fuel cells

Wei Xu [a], Xin Sun [a,*], Elizabeth Stephens [a], Ioannis Mastorakos [b], Mohammad A. Khaleel [a], Hussein Zbib [a,b]

[a] Pacific Northwest National Laboratory, Computational Sciences and Mathematics Division, P.O. Box 999, Richland, WA 99352, USA
[b] School of Mechanical and Materials Engineering, Washington State University, P.O. Box 642920, Pullman, WA 99164-2920, USA

HIGHLIGHTS

► A mechanistic-based two-stage model was developed to study the self-healing glass materials.
► Experimental healing measurements were conducted to characterize model parameters.
► Finite element-based healing analyses are presented for various healing conditions.

ARTICLE INFO

Article history:
Received 5 June 2012
Received in revised form
7 July 2012
Accepted 9 July 2012
Available online 17 July 2012

Keywords:
Solid oxide fuel cell
Glass seal
Self-healing
Mechanistic model
Finite element analysis

ABSTRACT

The use of self-healing glass as hermetic seals is a recent advancement in sealing technology development for the planar solid oxide fuel cells (SOFCs). Because of its capability to restore mechanical properties at elevated temperatures, the self-healing glass seal is expected to provide high reliability in maintaining the long-term structural integrity and functionality of SOFCs. To accommodate the design and evaluate the effectiveness of these engineered seals under various thermomechanical operating conditions, a computational modeling framework must be developed to accurately capture and predict the healing behavior of the glass material. In the present work, a mechanistic-based, two-stage model was developed to study the stress and temperature-dependent crack healing of the self-healing glass materials. The model initially was first calibrated by experimental measurements combined with kinetic Monte Carlo (kMC) simulation results and then implemented into finite element analysis (FEA). The effects of various factors, e.g., stress, temperature, and crack morphology, on the healing behavior of the glass were investigated and discussed.

1. Introduction

Planar solid oxide fuel cells (SOFC) represent a class of high-efficiency energy conversion devices that directly transform chemical energy into electrical energy via electrochemical oxidation without the emission of noxious gases compared to the combustion of fossil fuels. Hence, they are considered promising candidates for a stand-alone clean power resource [1]. As one of the most critical engineering components in the SOFC system, the hermetic gas sealant is responsible for preventing air and fuel leakage and isolating the fuel from the oxidant [2,3]. Its structural integrity and functionality are critical to the reliability and durability of SOFC stacks. Therefore, many efforts have been devoted to the research and development of reliable sealant materials and sealing system designs [4–6].

Mechanistically speaking, the seals currently in service can be categorized into two types: 1) compressive seals and 2) rigid seals [7,8]. Compressive sealing confines a compliant, high-temperature material in between two sealing surfaces by an external compression load frame, while rigid seals rely on the effective bonding between the sealant material and sealing surfaces. Major concerns with compressive sealing technology include the chemical and mechanical stability of the sealant materials under a highly reactive and elevated temperature environment, the proper design of the load frame, and the disadvantages of introducing an external compressive load frame into the SOFC stacks [9,10]—although recent studies on Al_2O_3-based compressive seals revealed the Al addition can significantly improve seal stability and reduce leakage rates [11,12]. In contrast, the family of rigid seals has become increasingly favorable.

* Corresponding author. Tel.: +1 509 372 6489; fax: +1 509 375 2604.
E-mail address: xin.sun@pnnl.gov (X. Sun).

0378-7753/$ – see front matter © 2012 Elsevier B.V. All rights reserved.
http://dx.doi.org/10.1016/j.jpowsour.2012.07.018

Among rigid seals, the high-temperature glass joining provides a low-cost and relatively simple method to bond ceramic and metal parts. However, its brittle nature at room temperature upon stack cooling generates significant concerns regarding its structural integrity during thermal cycling. The glass seal is particularly vulnerable to fracture when subjected to tensile stress. Hence, materials development efforts have focused on designing the thermal expansion coefficients of each stack components, including the ceramic cell, seal, and separator, to be approximately equal, thereby minimizing the buildup of thermal stress during thermal cycling [6,13,14].

Self-healing glass is a recent development of innovative hermetic glass sealant materials. It has the ability to restore its mechanical properties when heated to elevated temperatures, effectively repairing the cooling-induced cracking. The long-term geometric stability and thermomechanical behavior of the highly temperature-dependent self-healing glass under the stack operation conditions have been extensively investigated in previous works [6,15,16]. However, quantitative studies on its most essential feature—the damage-healing characteristics—are rarely reported in the open literature.

Conversely, engineering structural-scale damage and recovery has been computationally studied by many researchers using different modeling approaches. Microstructure-based damage models have been developed to account for the influence of the distribution, growth, and interactions of cracks and voids to macroscopic material behavior [17,18]. Mesoscale models are adopted to investigate interfacial debonding failure within composites [19]. Owing to recent developments in nano/micro systems, multiscale material modeling has emerged as a critical link in computational materials research [20,21]. Because the goal of many of these investigations is to determine the macroscopic structural performance, phenomenological-based continuum damage mechanics, which smears the micro-cracks/damages within the material with effective degraded properties, i.e., the strength, Young's modulus, etc., is frequently used [22–24]. Both damage and healing variables incorporated in this method are established based on the correlation between the behavior of individual cracks and the overall response of the material [25–28]. As a result, discrete models considering the exact crack details are needed to quantify the morphological evolution of the cracks and their effects on structural characteristics.

The self-healing characteristics of amorphous materials, such as polymers, have received a good deal of attention in recent years. The healing is defined as completed only when both the full re-establishment of the geometric continuity and the recovery of the mechanical strength are realized [29]. In other words, the whole crack healing process essentially consists of two locally sequential phenomenological stages: 1) crack closure and 2) crack healing [30]—a concept that has been verified by recent experimental findings in a shape memory polymer-based composite material [31–33]. Although various analytical and numerical models of the build-up of the joint strength between crack surfaces have been developed for the crack healing stage, the studies usually were limited to fundamental dimensionless analyses [34] in which the mechanical and geometrical inhomogeneity in the crack evolution process is not considered and is only applicable to specific loading conditions [35]. In addition, the effects of crack closure kinetics are rarely considered.

In this work, a mechanistic-based self-healing model is presented and incorporated into a numerical framework to quantitatively capture and predict the crack healing behavior of self-healing glass seals. The entire healing process is conceptually divided into two sequential stages: 1) crack closure and 2) crack healing. Crack closure is considered to be governed by the stress-driven viscous creep flow, while crack healing is perceived as an interfacial diffusion process characterized by a temperature-dependent dwelling time that can be predicted by the kinetic Monte Carlo (kMC) method. To obtain the model parameters, controlled healing experiments were conducted at different temperatures followed by four-point bending tests to evaluate the recovery of the material strength. Because healing experiments can only be conducted at selected temperatures with limited time increments, experimentally measured healing ratios at different temperatures are used to calibrate kMC model parameters. These parameters then are used for extrapolating the experimental results to a wider temperature range to formulate the temperature dependence of the characteristic dwelling time. Then, the proposed healing mechanisms were implemented into finite element models to simulate the self-healing behavior of the glass material under different thermomechanical conditions. Effects of various factors, such as temperature, stress, and crack characteristics, also were evaluated.

2. Two-stage healing mechanism

The actual crack morphology change observed in the healing process of glass materials typically includes crack tip blunting, ovulation, and shrinkage. The original continuous plane cracks are first cylindrically pinched off then evolve into spherical pores, which later recede before completely disappearing [36]. Considering that the essential driving force of the crack healing is to eliminate the fracture surface and reduce the associated surface energy, several underlying mechanisms have been proposed, including thermal annealing, intermolecular adhesion, and chemical reaction [37]. In the case of glass, it is believed that the capillarity-driven viscous flow and sintering process dominate the process [38].

Although different analytical models have been proposed to explain individual characteristic morphology changes during the healing process [39–41], a general framework to cover the entire healing process that considers multiple effects is still lacking. Furthermore, because the local crack morphological evolution at the fracture interface usually is unsynchronized and unordered, results from the models for individual cracks cannot be extended to multiple cracks by simple rule of linear superposition.

As discussed, because a complete crack healing relies on both free surface removal and intermolecular diffusion-based strength recovery, the local healing progress can be conceptually divided into two sequential phenomenological stages: 1) crack closure and 2) crack healing. For any infinitesimal fracture area dA, at elevated temperatures and under compressive stress conditions, viscous creep flow first will bring the two crack-free surfaces into contact. Once the physical constant is established, the mass transport across the crack interface, driven by surface interdiffusion, follows and gives rise to the re-establishment of the physical bonds between the crack surfaces, leading to gradual restoration of its mechanical strength. As the viscous deformation process depends on local thermomechanical conditions, the most common macroscopic crack healing path is expected to be discontinuous, involving jumps, voids, and irregular secondary cracks, as observed in experiments.

The viscous creep behavior in the crack closure stage can be evaluated by many mechanisms. Here, for the amorphous pure glass material, the linear creep constitutive law is adopted [42]:

$$\dot{\varepsilon} = \frac{1}{\eta}\sigma \tag{1}$$

where $\dot{\varepsilon}$ and σ are the local strain rate and stress, respectively, and η is temperature-dependent viscosity.

For the crack healing stage, the surface interdiffusion corresponding to the growth of the physical links between the fracture surfaces in intimate contact is assumed to be proportional to the average penetration depth of molecules [43]. According to Einstein diffusion equation, a characteristic dwelling time τ_0 is required to reach a critical interpenetration depth and establish enough interfacial bonds to fully recover the mechanical strength.

Because the diffusion processes are usually temperature-dependent, we then have:

$$\tau_0 = \tau_0(T) \tag{2}$$

which later can be formulated based on the experimental measurements. It should be noted that, in reality, the mass diffusivity also can be dependent on stress and chemical conditions. However, because the primary aim of this work is to establish a framework to investigate the crack healing behavior of the glass sealant material, only temperature dependence is considered herein for demonstration purposes.

3. Experiment

Rectangular SCN-1 self-healing glass bar specimens with dimensions of 4 mm × 3 mm × 23 mm were prepared for experimental testing. For the given bar geometry, SCN-1 glass powder was uniaxially die-pressed then sintered. The bar specimens were first exposed to 550 °C for two hours then exposed to 700 °C for three hours and finally cooled to room temperature.

In the controlled healing experiments, two bars were placed vertically in a fixture as shown in Fig. 1 and exposed to elevated temperatures. The stainless-steel fixture is oxidized and has a black/purplish tint. To prevent binding during the heat-treating process, mica was used in the fixture's interior and all mating surfaces with the glass. Since no gap is left between the specimens, the two bars together can be perceived as one SCN-1 glass bar of double length but with an already closed cross-sectional crack in the middle of the span. The healing experiments actually record the fracture surface interdiffusion and physical bonding re-establishment evolution in the healing stage.

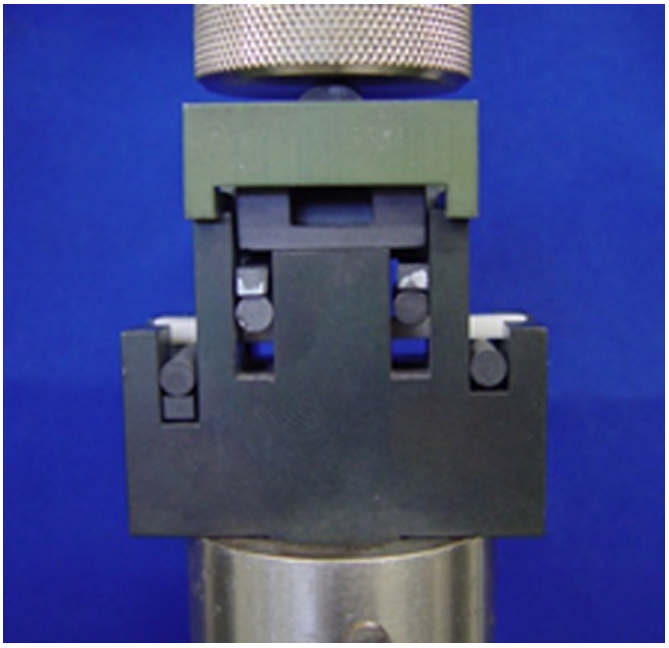

Fig. 2. Four-point flexural test set-up.

In the healing experiments, the specimens were exposed to varying time periods at each elevated temperature. Their corresponding post-healing, ambient temperature flexural strength was then measured via four-point flexural tests following ASTM

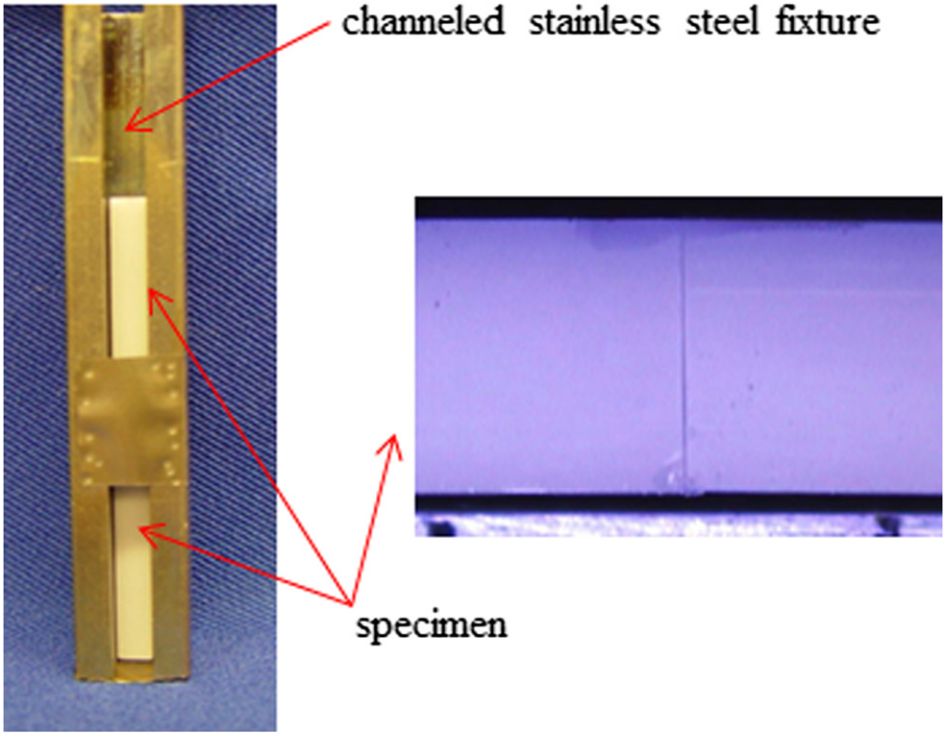

Fig. 1. Image of two glass bars placed vertically into the channeled test fixture.

standard C1161-02 procedures. The flexural test set-up is shown in Fig. 2, where a 40-mm outer span and a 20-mm inner span were used.

Fig. 3 shows a typical post-healing specimen. It is found that the original interface between the two bars has completely disappeared, although the width at the original interface location slightly changes probably due to the sintering process. The post-healing strength measurements for healing temperatures of 700 °C and 800 °C are listed in Table 1 for various dwelling time. The specimens' strength is shown to generally increase as the duration increases at the elevated temperature environment. According to our proposed interdiffusion driven healing mechanism, this observed behavior is expected. In addition, it appears that higher temperature accelerates the healing process. As discussed previously, the material strength recovery is considered to be linearly proportional to the re-establishment of the physical bonds across the fracture interface. Then, the evolution of the healing stage can be described through a non-dimensional term, the broken bond ratio (r_b), given as:

$$r_b = 1 - \frac{S}{S_0} \tag{3}$$

where S is the measured flexural strength and S_0 is the strength of the intact SCN-1 glass, which is around 80 MPa based on the measurements.

4. kMC simulation for characteristic dwelling time calibration

kMC, a computational tool for studying the breaking and healing of bonds in materials, originates from radiation damage annealing studies of an atomistic system in the early 1960s [44]. With its main advantage over molecular dynamics simulations as the longer simulation time scale, kMC is commonly used as an effective tool in simulating the time evolution of natural physical processes, for example, the interdiffusion healing stage in the current study. Here, the kMC model will first be calibrated by the controlled experimental results. Then, its predictions will be used to extrapolate the experimental measurements to a wider temperature range and formulate the temperature-dependent functional form of the characteristic dwelling time, which will be adopted in the finite element simulation to determine if and when the segments of the crack surfaces are to be re-bonded.

Fig. 4 shows the two-dimensional (2-D), geometrically non-dimensional lattice model used in the kMC simulation in this study, where the lattice spacing Δx denotes one unit length. The microstructure specimen is an $(M \times \Delta x) \times (M \times \Delta x)$ square, and the central rectangular hole is $M/2 \times \Delta x$ long and $1\Delta x$ wide. If Δx takes the covalent bond length of the glass, the model actually represents a specimen with an already closed but not healed crack. To ensure the accuracy of the characteristic dwelling time prediction, $M = 1000$ is used in the following simulations (after careful convergence studies).

Table 1
Flexural tests results summary for specimens exposed to elevated test temperatures with no gap at the interface and no load.

Healing test temperature (°C)	Dwelling time at healing test temperature (min)	Ambient temperature flexural strength (MPa)
700	40	23
700	60	51.7
700	120	79.8
800	5	10.5
800	10	66.8
800	20	75.5

The probability of a bond to be healed is considered to be governed by:

$$P = w_h{}^* \exp\left(-\frac{E_h}{kT}\right) \tag{4}$$

where k is Boltzmann constant, w_h is the frequency and E_h is the activation energy. Because we currently assume the diffusion process to be solely dependent on temperature, the effects of external pressure are not considered here, although they can be further included into the model following a similar method as discussed by Zhao et al. [45]. Fig. 5 shows a typical example of the structure healing process. It is clear that all of the broken vertical bonds in the original cracked specimen (Fig. 4) are gradually re-established.

Here, the broken bond ratio r_b evaluating the crack healing performance can be directly calculated by the ratio of the number of remaining broken bonds to the initial number of broken bonds, where the broken bonds denote the missing vertical grid between the crack surfaces. From a typical healing curve shown in Fig. 6, it can be seen that the bond reformation process propagates rather fast initially, while it gradually slows down as the broken bond ratio approaches zero, which indicates complete healing. The total evolution time represents the necessary time period to fully reinstate the physical bonding between the fracture surfaces. Therefore, it measures the characteristic dwelling time.

The formulation of the temperature-dependent characteristic dwelling time follows a two-step calibration procedure. First, experimental measurements at 700 °C and 800 °C are used to calculate the broken bond ratio following Equation (3). Then, they are used to calibrate the kMC model parameters: activation energy (E_h) and frequency (w_h). As shown in Fig. 7, a reasonable fit is reached when $E_h = 2.555$ eV and $w_h = 6.02\text{E}9$ Hz.

Next, the calibrated kMC model is used to predict the bond reforming evolution under a wider range of temperature conditions to establish a mathematic formulation for the temperature-dependent characteristic dwelling time.

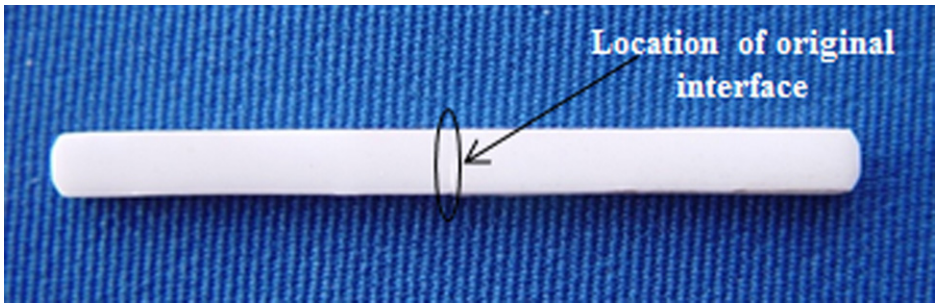

Fig. 3. Specimen exposed to 700 °C for 60 min with no load and no gap at the interface.

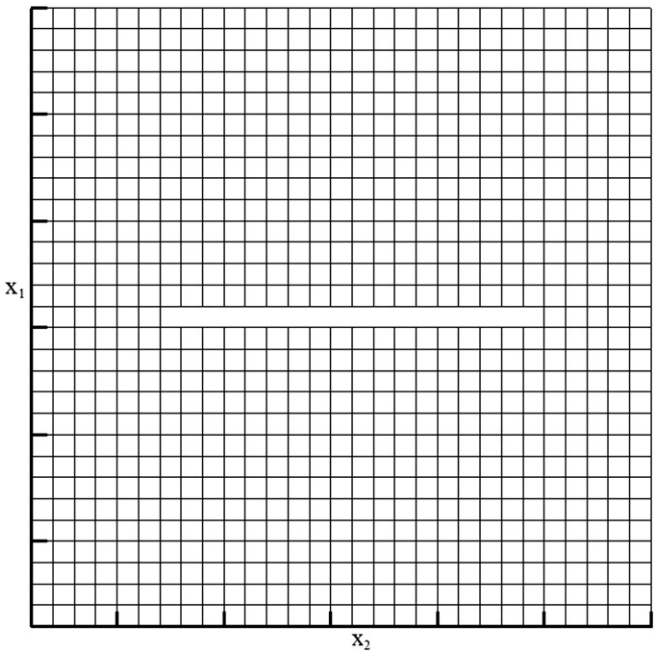

Fig. 4. The kMC model for diffusion-driven cracking healing.

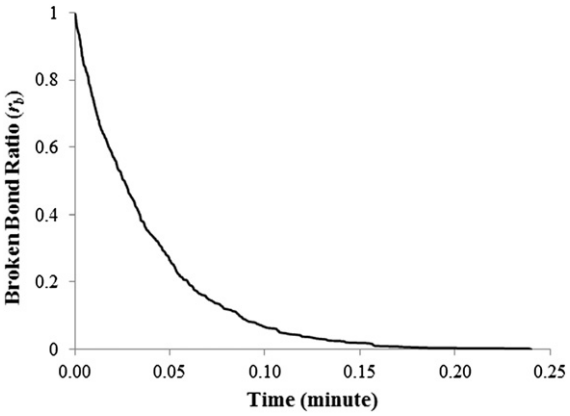

Fig. 6. The evolution of the broken bond ratio captured by the kMC simulation.

An Arrhenius-type functional form is proposed to fit the kMC prediction results as follows:

$$\tau_0(T) = \alpha \exp\left(\frac{\beta}{T}\right) \tag{5}$$

where τ_0 is in minute and T is in Kelvin. Through a MATLAB optimization routine, $\alpha = 2.4082\text{E-}9$ and $\beta = 24{,}890$ are found to provide the best fit, as shown in Fig. 8. This functional relation was next incorporated into the proposed two-stage healing mechanistic model and implemented into the finite element simulations through user subroutines. It should be noted here that the primary aim of the controlled experimental measurement is to calibrate the kMC model rather than quantitatively validate it. Although the two crack surfaces are kept in full contact macroscopically to mimic the healing of a closed crack in the controlled experiments, in practice there might still be some micro gaps left on the interface, which may lead to the differences between the experimental measurements and kMC predictions. Moreover, the probability function used in the kMC model is assumed to be solely temperature dependent, which also may introduce deviations from reality.

5. Simulations of the two-stage healing process with finite element method

The finite element analysis (FEA) simulation was performed using the commercial finite element software package, ABAQUS. A 100 mm × 100 mm 2-D plane strain numerical model with a 10-mm-long V-type edge crack (as shown in Fig. 9) is used to represent the cross section of a glass sealant. The crack tip opening considered here is 0.1 mm. All displacements of the bottom side are fixed, and a uniform pressure is applied on the top surface, resulting in a mode-I crack. Gravity effect of the material is also included.

Other than the characteristic dwelling time (as calibrated in the previous section), the thermal and mechanical properties of the SCN-1 glass were obtained from the open literature. The temperature-dependent Young's modulus shown in Fig. 10 was partially measured experimentally by Oak Ridge National Laboratory (ORNL) [46]. Because the testing method is no longer valid when the temperature exceeds the glass transition temperature,

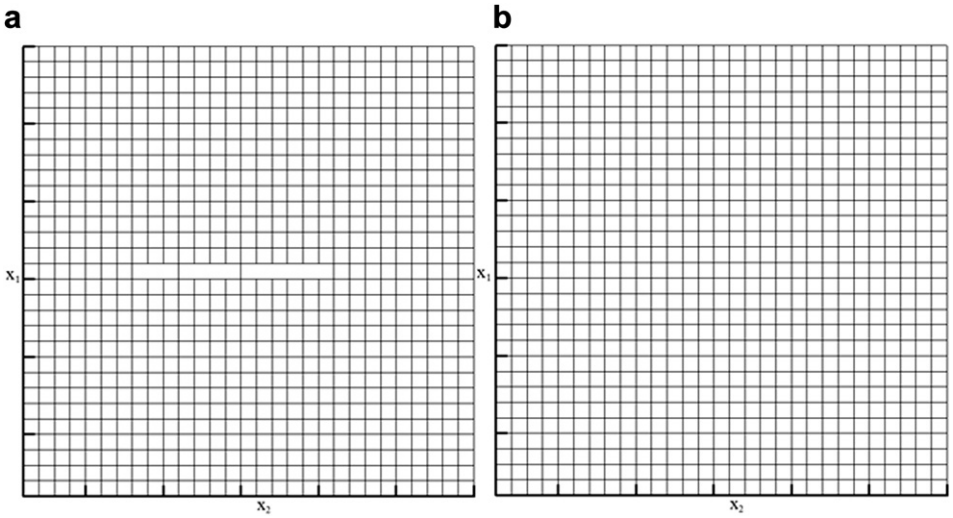

Fig. 5. A typical example of the structure healing process in the kMC simulation: (a) partially healed structure and (b) completely healed structure.

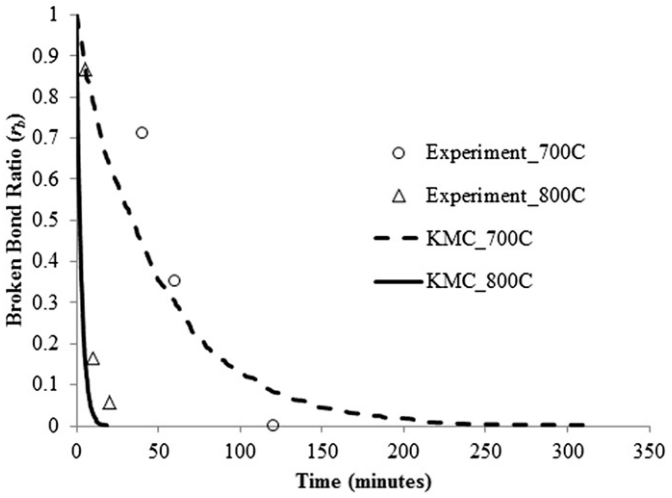

Fig. 7. kMC model calibration.

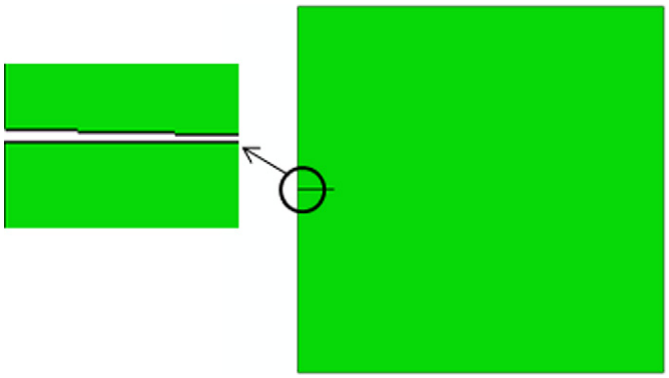

Fig. 9. Finite element model with the horizontal V-type edge crack.

i.e., the T_g of the SCN-1 glass, the modulus values for temperatures beyond T_g were extrapolated [6] in a manner consistent with typical glass behavior [47,48].

Fig. 11 shows the temperature-dependent coefficient of thermal expansion (CTE) data within the temperature range of interest [3].

The viscosity measurements of SCN-1 glass also were performed at ORNL. Isothermal creep tests under three different constant loads were conducted at high temperatures between 600 °C and 850 °C with a heating rate of 5 °C min^{-1} [49]. It is assumed that the temperature-dependent viscosity for the glass follows a typical Arrhenius equation:

$$\eta = \eta_0 \exp\left(\frac{Q_v}{RT}\right) \tag{6}$$

where $R = 8.314$ $JK^{-1}mol^{-1}$ is the universal gas constant, Q_v is the activation energy, and η_0 is the reference viscosity. The parameters for SNC-1 self-healing glass were determined from experimental measurements as $\eta_0 = 1.397 \times 10^{-9}$ Pa s and $Q_v = 283.32$ kJ mol^{-1}.

The two-stage healing mechanism described in the previous sections is then implemented into ABAQUS through user subroutines. The initial crack surfaces are considered to be free surfaces with no interaction constraints. When segments of the two crack surfaces are driven into contact by the viscous flow and remain in contact for a period of the characteristic dwelling time corresponding to the environmental temperature, rigid sticking interaction condition is applied to restrict the relative movements and to represent the full establishment of the molecular physical bonding across the fracture interface.

Fig. 12 shows the structure after undergoing healing at 1000 °C under 5 MPa pressure for ~17 min. After healing, the crack is shown completely closed. The concentration of the creep strain in the vertical direction near the crack edge further indicates that geometric crack closure is due to growing viscous creep deformation.

Before healing, the interaction between the initial crack surfaces is assumed to be frictionless. Therefore, no tangential constraints can be transmitted across the fracture interface—even for a fully closed crack. As such, the non-zero interfacial shear stresses along the crack interface in the post-healing structure (shown in Fig. 13) indicate that the crack not only has been fully closed but also completely healed.

The evolution of the crack closure and healing can be evaluated with two non-dimensional parameters: crack closure ratio ($r_{closure}$) and crack healing ratio (r_{heal}), respectively, given by:

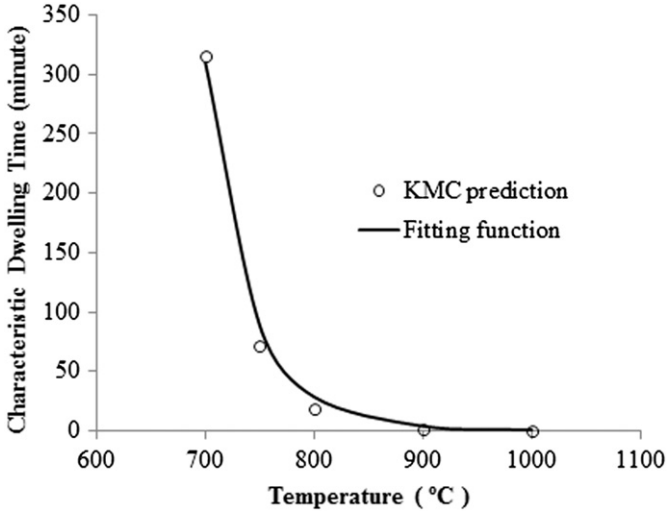

Fig. 8. Calibration of the temperature dependent dwelling time.

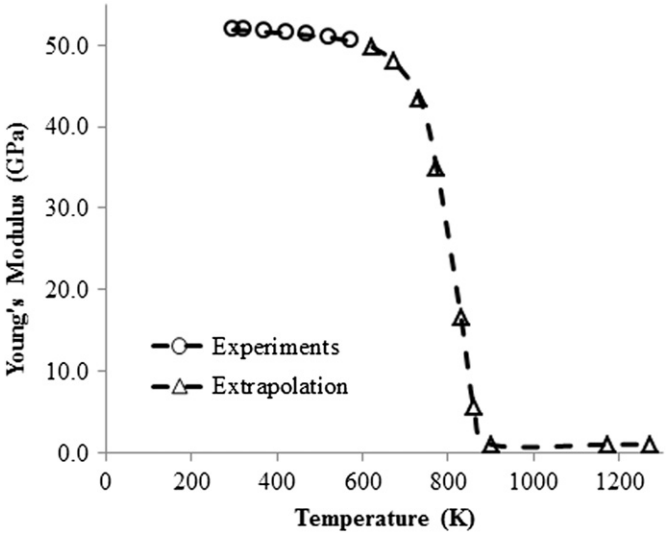

Fig. 10. Temperature-dependent Young's modulus of the SCN-1 glass.

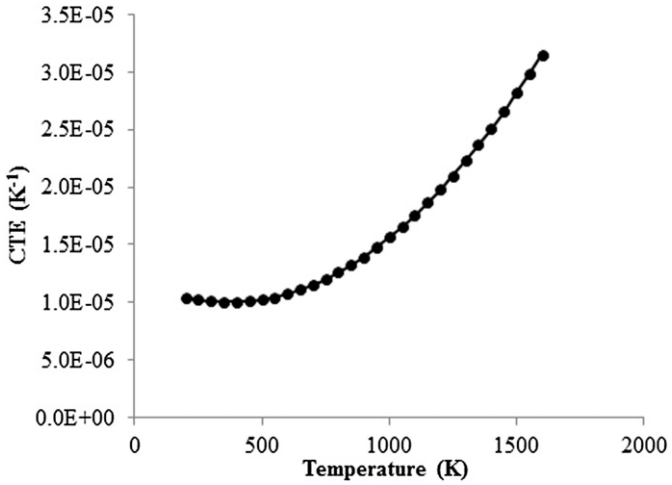

Fig. 11. Temperature-dependent CTE of the SCN-1 glass.

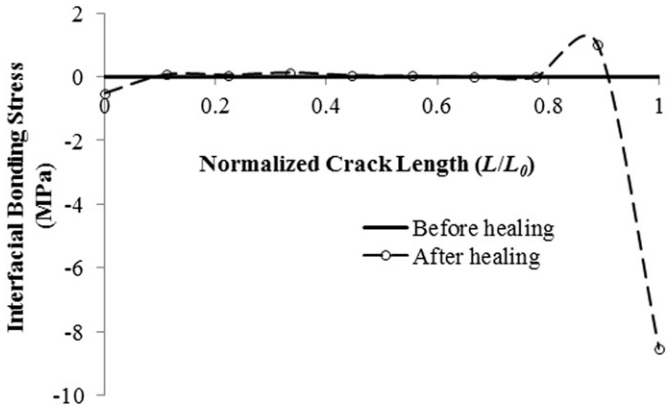

Fig. 13. Interfacial bonding stress along the healed crack interface.

$$r_{\text{closure}} = \frac{l_{\text{closed}}}{l_0} \tag{7}$$

$$r_{\text{heal}} = \frac{l_{\text{healed}}}{l_0} \tag{8}$$

where l_0, l_{closed}, and l_{healed} correspond to the initial crack length, closed crack length, and healed crack length, respectively.

As shown in Fig. 14, it is clear that crack healing always lags behind crack closure. The time lag captured by the simulation is 0.75 min, less than 1 min, which coincides with the characteristic dwelling time at 1000 °C determined from Equation (5), confirming the correct implementation of the proposed mechanistic model.

5.1. Effects of healing temperature

To investigate the effect of the operating temperature on the healing behavior, different temperature field conditions were applied to the model. Fig. 15 shows the variation of the total healing time (the sum of the duration of both crack closure and healing stages) versus temperatures and its comparison with the temperature-dependent variation of the characteristic dwelling time, which represents the intrinsic healing time for initially closed cracks.

Similar to the temperature dependence of the dwelling time, the total healing time is shown to increase as the temperature decreases, indicating that lower temperatures reduce the healing rates. This is due to the fact that both crack closure and healing are thermally driven processes. When the temperature further decreases and approaches the glass transition temperature, the molecular mobility is greatly reduced, leading to a sharp decrease in the diffusion rate and a drastic increase in viscosity. As a result, both crack closure and healing processes prolong. Moreover, at high temperatures (>800 °C), the total healing time is found to be determined mostly by the crack closure time. The cracks almost instantly heal once the crack surfaces come into contact. Meanwhile, at low temperatures (<800 °C), the considerably low diffusion rate becomes a more dominant effect. For the states of stress that have been studied, the predicted results further indicate that a small reduction in the operating temperature will not likely to lead to a drastic increase in healing time. For example, the healing time at 900 °C is 20 min and at 850 °C is 26 min.

5.2. Effects of stress conditions

The stress effect on the healing performance also is studied by applying different amounts of pressure onto the top surface of the model. A stress factor, defined as the total healing time under

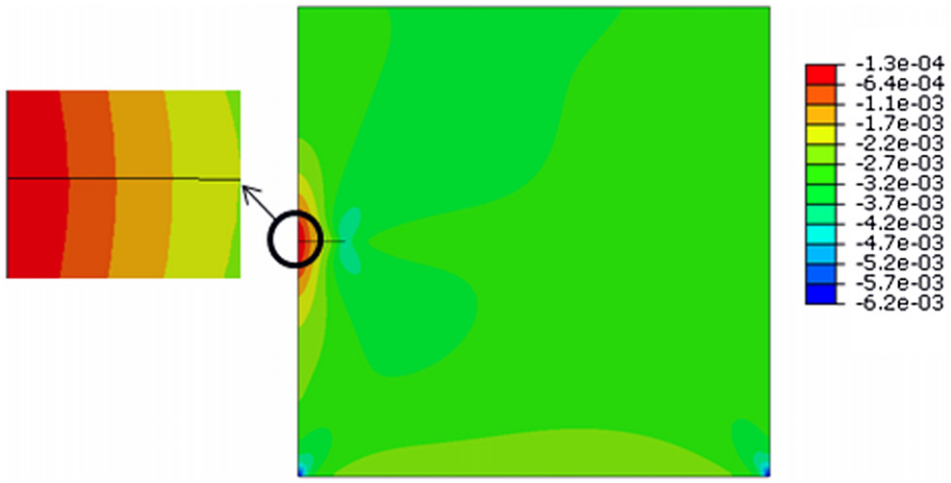

Fig. 12. Healed structure at 1000 °C in the FEA simulation: creep strain contours.

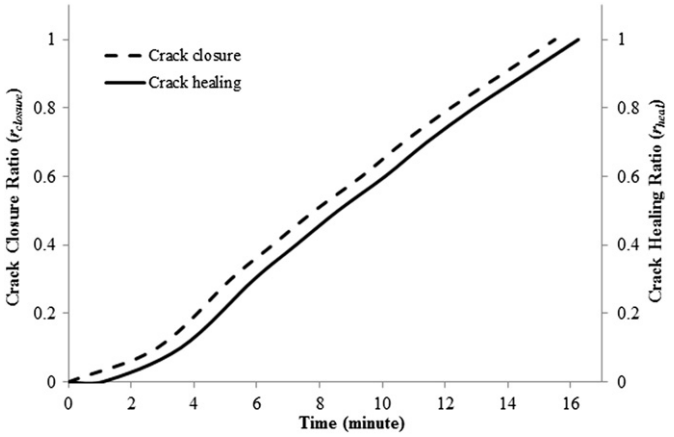

Fig. 14. The evolution of crack closure and crack healing at 1000 °C.

10 MPa divided by the total healing time under 5 MPa, is calculated to quantify the stress-induced variation in healing efficiency. The stress effect at different operating temperatures is shown in Fig. 16.

It is found that higher confining stress generally shortens the healing process. However, as the temperature decreases, the stress-induced healing efficiency enhancement becomes less effective. Because the external stress primarily affects viscous creep behavior, this finding also is consistent with the results shown in Fig. 15 and illustrates that the influence of the crack closure stage on the total healing time is comparatively decreasing at lower temperatures.

5.3. Effects of crack orientation

To investigate the effects of crack characteristics, i.e., mode mix, on the healing behavior, V-type edge cracks with the same length and opening width but different orientations are introduced to the model. The crack orientation θ is defined as the angle between the loading direction and the crack length direction as shown in Fig. 17. When θ is equal to 90°, the crack is initially a mode-I crack. Otherwise, it is a mixed-mode crack, i.e., mode-I and mode-II crack.

The specimens are considered to be healed under 5 MPa pressure at 850 °C. The orientation effects were evaluated by the orientation factor, expressed by $t/t(\theta = 90°)$, where t is the total healing time and $t(\theta = 90°)$ represents the total healing time for a specimen with a crack of $\theta = 90°$.

The dependence of the orientation factor on crack orientation is shown in Fig. 18. As the crack orientation deviates from the

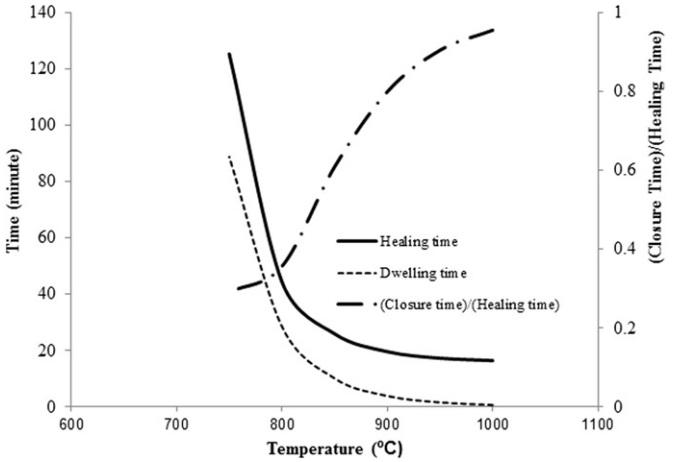

Fig. 15. Effects of operating temperatures on the healing performance.

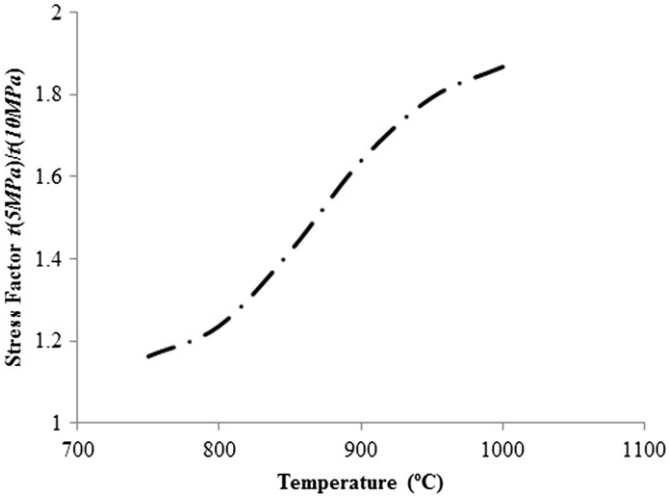

Fig. 16. Effects of stress conditions on the healing performance.

direction normal to the local compressive stresses, the healing time is shown to increase drastically. This suggests that when establishing the damage-healing criteria to evaluate the performance of the self-healing glass seals under complicated stress conditions, both local stress magnitude and direction (mode mix) should be taken into account. The predicted results can be further used to formulate the healing variable in future continuum damage-healing model development.

5.4. Effects of crack interaction

It is well known that interactions among multiple cracks can strongly affect the local stress field and influence crack propagation [17,50]. To determine their effects on crack-healing behavior, an extra V-type edge crack of the same dimension was introduced into

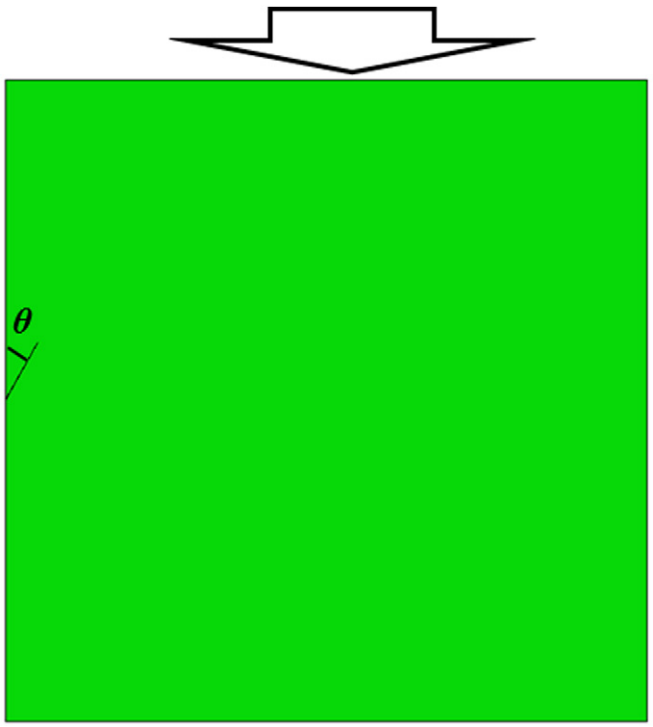

Fig. 17. Finite element model with the V-type edge crack of an arbitrary orientation.

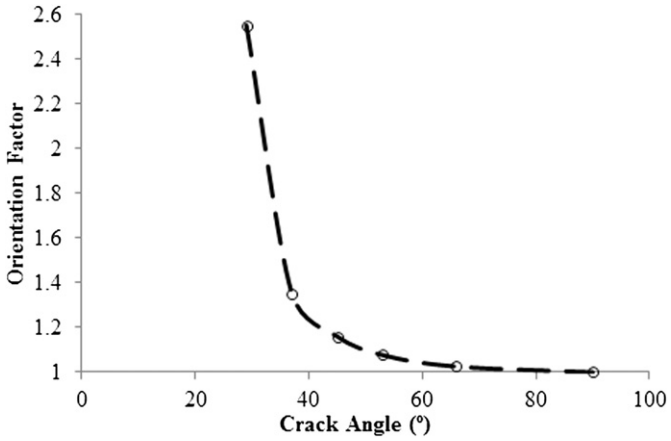

Fig. 18. Effects of local stress conditions and crack morphology on the healing performance.

the model (as shown in Fig. 19). A dimensionless distance d, given by D/l_0 where D represents the actual distance between the new crack and the original one, was used to estimate the distribution of the cracks.

Fig. 20 shows the effects of the crack–crack interaction on crack healing at 850 °C. The interaction effects were evaluated by a non-dimensional interaction factor, given by $t/t(D = \infty)$ where t is the total healing time and $t(D = \infty)$ is the total healing time for the specimen with a single crack. The presence of an additional crack significantly elongates the healing process. Moreover, when cracks get closer, the healing time increases rather nonlinearly. It indicates that in addition to the number of the cracks, the crack distribution also appears to be crucial to the damage-healing performance. In reality, as a large number of cracks can be even more closely surrounded by each other, one can expect that the interference of the multiple cracks eventually may lead to crack pileup, kinking, and coalescence. Their impact on the healing behavior must be further investigated.

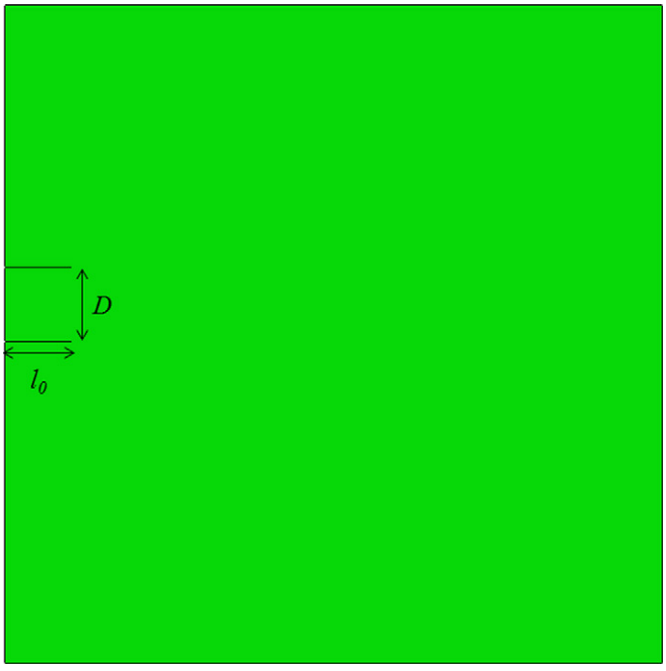

Fig. 19. Finite element model with two cracks.

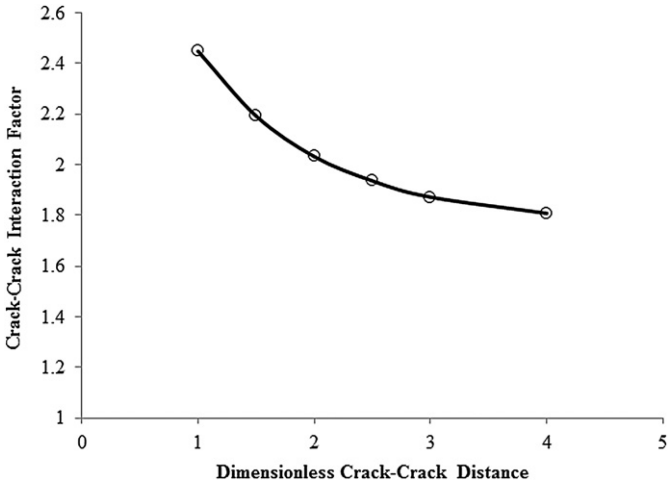

Fig. 20. Effects of crack–crack interaction on the healing performance.

6. Conclusions

A mechanistic-based healing model was developed for the self-healing glass SOFC sealant material in this study. The local healing process was conceptually divided into two sequential phenomenological stages: 1) crack closure and 2) crack healing. Viscous creep flow is considered to be responsible for the crack closure, while the surface interdiffusion at the closed crack interface is believed to dominate crack healing. Controlled healing experiments at elevated temperatures followed by four-point flexural tests were conducted to assess the structural healing performance. kMC simulations based on the diffusion-induced crack healing mechanism were performed and used to calibrate the proposed mechanistic model with the aid of the experimental measurements. The healing mechanism was then implemented into the FEA. Effects of various thermomechanical conditions and crack morphology on the healing behavior were examined. Based on the simulation results, the following observations and conclusions can be made:

1) High temperature leads to faster healing. For the cases considered here, the total healing time is mostly determined by the crack closure stage at extremely high temperatures (>800 °C) when the cracks instantly heal as the crack surfaces come into contact, while it is primarily dominated by the crack healing stage at low temperatures (<800 °C) when diffusion is considerably slow.
2) External confining stresses help accelerate crack healing. However, such influence becomes less effective as the temperature decreases because the stress primarily takes effect in the crack closure stage, which is less influential on the total healing time as temperature decreases.
3) Both the magnitude and directions of the local stresses affect the viscous flow around the crack and the healing behavior. The healing time drastically increases as the crack orientation (θ) deviates from the direction normal to the applied compressive stress ($\theta = 90°$) while asymptotically reaching a plateau as it approaches 90°.
4) The presence of multiple cracks increases the healing time. As cracks get closer, the adverse effects on the healing behavior induced by the crack–crack interaction appear to be more significant.

However, *in situ* video imaging experimental observations of the glass' self-healing response suggest that, in reality, a mixed

combination of mechanisms actually are involved in the healing process, e.g., viscous flow sintering dominates the blunting of the crack tips and capillary force primarily governs the filling of the crack cavity [39]. Reduction of the total free surface energy of the system is believed to be the fundamental driving force [51]. Therefore, a true healing process may not be fully represented by any single mechanism. To fully account for the contributions from all of the mechanisms, a more comprehensive healing model needs to be developed. The essential purpose of the present study is to outline a mechanistic framework to describe the self-healing mechanism of self-healing glass sealant materials. Although the model may not be precisely calibrated, the concept and methodology can still be used to model the healing behavior and estimate the effects of the operating conditions on the healing performance.

It also should be noted that the material characteristic dwelling time here is assumed to be solely dependent on the temperature (for simplicity). However, in practice, it is possible that the interdiffusion process also can have dependence on stress, chemical, or aging effects. Moreover, in the current study, the effect of the crack surface morphology was not considered [43]. Because another purpose of the discrete crack healing model is to provide the missing links between the behavior of the individual cracks and the overall structural response for the upscale continuum damage-healing modeling and SOFC stack-level simulation, additional factors, such as the density and distribution of multiple cracks, need to be considered in future studies.

Acknowledgments

The work presented in this paper was funded as part of the Solid-State Energy Conversion Alliance Core Technology Program by the U.S. Department of Energy's (DOE) National Energy Technology Laboratory. Pacific Northwest National Laboratory is operated by Battelle for DOE under contract DE-AC05-76RL01830.

References

[1] T. Iwata, Y. Enami, Journal of The Electrochemical Society 145 (1998) 931–935.
[2] R.N. Singh, Journal of Materials Engineering and Performance 15 (2006) 422–426.
[3] N. Govindaraju, W.N. Liu, X. Sun, P. Singh, R.N. Singh, Journal of Power Sources 190 (2009) 476–484.
[4] K.S. Weil, B.J. Koeppel, International Journal of Hydrogen Energy 33 (2008) 3976–3990.
[5] W.N. Liu, X. Sun, M.A. Khaleel, Journal of Power Sources 185 (2008) 1193–1200.
[6] W.N. Liu, X. Sun, M.A. Khaleel, Journal of Power Sources 196 (2011) 1750–1761.
[7] J.W. Fergus, Journal of Power Sources 147 (2005) 46–57.
[8] R.N. Singh, International Journal of Applied Ceramic Technology 4 (2007) 134–144.
[9] S.P. Simner, J.W. Stevenson, Journal of Power Sources 102 (2001) 310–316.
[10] Y. Chou, J.W. Stevenson, L.A. Chick, Journal of Power Sources 112 (2002) 130–136.
[11] S. Sang, W. Li, J. Pu, L. Jian, Journal of Power Sources 177 (2008) 77–82.
[12] Z. Dai, J. Pu, D. Yan, B. Chi, L. Jian, International Journal of Hydrogen Energy 36 (2011) 3131–3137.
[13] W.N. Liu, X. Sun, E. Stephens, M.A. Khaleel, Journal of Power Sources 189 (2009) 1044–1050.
[14] W.N. Liu, X. Sun, M.A. Khaleel, J.M. Qu, Journal of Power Sources 192 (2009) 486–493.
[15] W.N. Liu, X. Sun, B. Koeppel, M. Khaleel, International Journal of Applied Ceramic Technology 7 (2010) 22–29.
[16] J. Milhans, D.S. Li, M. Khaleel, X. Sun, M.S. Al-Haik, A. Harris, H. Garmestani, Journal of Power Sources 196 (2011).
[17] I. Demir, H.M. Zbib, M. Khaleel, Theoretical and Applied Fracture Mechanics 36 (2001) 147–164.
[18] L. Tashman, E. Masad, D. Little, H. Zbib, International Journal of Plasticity 21 (2005) 1659–1685.
[19] X.Z. Lu, L.P. Ye, J.G. Teng, J.J. Jiang, Engineering Structures 27 (2005) 564–575.
[20] J.D. Lee, X.Q. Wang, Y.P. Chen, Theoretical and Applied Fracture Mechanics 51 (2009) 33–40.
[21] G.C. Sih, X.S. Tang, Theoretical and Applied Fracture Mechanics 42 (2004) 1–24.
[22] N. Nguyen, B.J. Koeppel, S. Ahzi, M.A. Khaleel, P. Singh, Journal of the American Ceramic Society 89 (2005) 1358–1368.
[23] M.A. Khaleel, H.M. Zbib, E.A. Nyberg, International Journal of Plasticity 17 (2001) 277–296.
[24] M.B. Taylor, H.M. Zbib, M.A. Khaleel, International Journal of Plasticity 18 (2002).
[25] E. Masad, L. Tashman, D. Little, H. Zbib, Mechanics of Materials 37 (2005) 1242–1256.
[26] G.Z. Voyiadjis, A. Shojaei, G. Li, International Journal of Plasticity 28 (2012) 21–45.
[27] G.Z. Voyiadjis, A. Shojaei, G. Li, International Journal of Plasticity 27 (2011) 1025–1044.
[28] G. Voyiadjis, A. Shojaei, G. Li, P.I. Kattan, Proceedings of the Royal Society A: Mathematical, Physical and Engineering Sciences 468 (2012) 163–183.
[29] M.D. Hager, P. Greil, C. Leyens, S. Van-der-Zwaag, U.S. Schubert, Advanced Materials 22 (2010) 5424–5430.
[30] G. Li, N. Uppu, Composites Science and Technology 70 (2010) 1419–1427.
[31] J. Nji, G. Li, Polymer 51 (2010) 6021–6029.
[32] G. Li, D. Nettles, Polymer 51 (2010) 755–762.
[33] W. Xu, G. Li, International Journal of Solids and Structures 47 (2010) 1306–1316.
[34] Y.H. Kim, R.P. Wool, Macromolecules 16 (1983) 1115–1120.
[35] T.A. Plaisted, S. Nemat-Nasser, Acta Materialia 55 (2007) 5684–5696.
[36] B.A. Wilson, E.D. Case, Journal of Materials Science 32 (1997) 3163–3175.
[37] L. Jun, Z.X. Zheng, H.F. Ding, Z.H. Jin, Fatigue & Fracture of Engineering Materials & Structures 27 (2004) 89–97.
[38] H.D. Ackler, Journal of the American Ceramic Society 81 (1998) 3093–3103.
[39] G. Pallares, A. Grimaldi, M. George, L. Ponson, M. Ciccotti, Journal of the American Ceramic Society 94 (2011) 2613–2618.
[40] M.K. Schwiebert, W.H. Leong, IEEE Transactions on Components, Packaging, and Manufacturing Technology-Part C 19 (1996) 133–137.
[41] G. Bandyopadhyay, J.T.A. Roberts, Journal of the American Ceramic Society 59 (1976) 415–419.
[42] R.M. Trejo, Y. Wang, A. Sides, A. Shyam, E. Lara-Curzio, in: NETL Review Meeting, Richland, WA, 2009.
[43] K. Jud, H.H. Kausch, J.G. Williams, Journal of Materials Science 16 (1981) 204–210.
[44] J.R. Beeler- Jr., R.A. Johnson, Physical Review 156 (1967) 677–684.
[45] H. Zhao, D.E. Makarov, G.J. Rodin, International Journal of Fracture 167 (2011) 147–155.
[46] E. Lara-Curzio, A. Shyam, R.M. Trejo, Y.L. Wang, in: Technical Report, Oak Ridge National Laboratory, 2009.
[47] E.L. Bourhis, P. Gadaud, J.P. Guin, N. Tournerie, X.H. Zhang, J. Lucas, T. Rouxel, Scripta Materialia 45 (2001) 317–323.
[48] J.P. Andrews, Proceedings of the Physical Society of London 37 (1924) 169–177.
[49] W.N. Liu, X. Sun, E.V. Stephens, M.A. Khaleel, in: SECA Topical Report, Pacific Northwest National Laboratory, 2010.
[50] B. Chen, D. Gross, Wave Motion 26 (1997) 69–83.
[51] J.W. Bullard, Journal of Applied Physics 81 (1997) 159–168.